Chapter 23

Future Applications of Artificially-Synthesized Organic Molecules Containing Transition-Metal Atoms

Selma Mayda[1,2], Zafer Kandemir[1] and Nejat Bulut[1]

[1]*Department of Physics, Izmir Institute of Technology, Urla, Turkey,* [2]*Department of Materials Science and Engineering, Izmir Institute of Technology, Urla, Turkey*

23.1 INTRODUCTION

Artificially-synthesized organic molecules which contain transition-metal atoms offer new opportunities for applications in the electronics, pharmaceutical, and chemical industries. In this respect, it is interesting to note that these kinds of molecules already exist and are used widely in nature. For example, about one third of proteins and enzymes contain metal atoms [1−4], which are called metalloproteins and metalloenzymes. These molecules, which have been developed by evolution, play an essential role in the chemical reactions taking place in all organisms. In this article, we will discuss the electronic properties of metalloproteins and metalloenzymes with the purpose of using what we learn here in the design of new artificially-synthesized organic molecules.

We study the electronic properties of metalloproteins and metalloenzymes by using the framework of the Haldane−Anderson model of a transition-metal impurity in a semiconductor host material [5,6]. In particular, as an example for metalloenzymes we study the electronic structure of vitamin B_{12}, which contains a cobalt atom and also has an energy gap in the excitation spectrum as in a semiconductor. We use the combined Hartree−Fock (HF) and quantum Monte Carlo (HF + QMC) methods, as well as the combined density functional theory (DFT) and QMC (DFT + QMC) methods. Our results show that new electronic states, which are named impurity bound states (IBS), are formed in these molecules and they play an important role in determining the low-energy electronic properties. We see that small changes in occupancy of IBS lead to important changes in the electronic state and the magnetic correlations.

We also study the electronic properties of the Ru-based dye molecules which are used in dye-sensitized solar cell applications. In these dye molecules, the local atomic environment around the transition-metal atom is similar to those in the metalloproteins and metalloenzymes. We have performed DFT + QMC calculations for the Ru-based dye molecules and we find that the IBS also exists in them and might be playing an important role in the functioning of these molecules.

In view of our results, we think that the IBS will also play a central role in the electronic structure and functioning of new artificially-synthesized organic molecules. Hence, we suggest that the magnetic and electronic properties of the IBS can be exploited in the design of new synthetic catalyzers and enzymes, or other functional molecules. Such molecules may be utilized in electronics, chemical, and pharmaceutical industries.

23.1.1 Molecular Structure of Vitamin B_{12}

Vitamin B_{12}, which contains a Co transition-metal atom, is an example of a metalloenzyme. It is important in the production of the red blood cells and in the functioning of the nervous system, in addition to taking place in various other chemical reactions. The vitamin B_{12} has three known cofactors. They are cyanocobalamin (CNCbl), adenosylcobalamin (AdoCbl), and methylcobalamin (MeCbl). Here, we will concentrate on CNCbl which contains 181 atoms. Its molecular structure is shown in Fig. 23.1A.

In our studies on CNCbl molecule, we have first performed HF + QMC calculations for a simplified, truncated molecule (Im-[Co^{III} (corrin)]-CN^{+}) containing 56

Handbook of Nanomaterials for Industrial Applications. DOI: https://doi.org/10.1016/B978-0-12-813351-4.00024-9

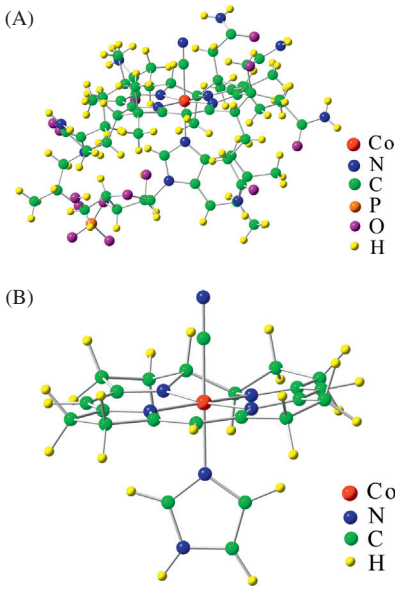

FIGURE 23.1 (A) Molecular structure of CNCbl ($C_{63}H_{88}CoN_{14}O_{14}P$). (B) Truncated molecular structure for Im-[Co^{III} (corrin)]-CN^{+}. *CNCbl*, cyanocobalamin.

atoms [5], which is illustrated in Fig. 23.1B. In these calculations, we have used the multiorbital Haldane–Anderson model but we neglected the interorbital Coulomb interactions. Next, we have performed DFT + QMC calculations for the full CNCbl molecule with 181 atoms included but without including the interorbital Coulomb interactions [6]. Finally, we have also performed DFT + QMC calculations for the full CNCbl molecule including the interorbital Coulomb interactions along with the Hund's coupling. In all of these three different computational approaches, we have observed the existence of the IBS and that it controls the magnetic correlations in CNCbl. Here, we find that the existence of the IBS is robust for CNCbl. Below in Sections 23.2.1 and 23.2.2, we will discuss the results from the HF + QMC for the truncated molecular structure without interorbital Coulomb interactions and also from the DFT + QMC for the full CNCbl including the interorbital Coulomb interactions.

23.1.2 Molecular Structure of the Ru-based Dye Molecules

Ru-based dye molecules which are used in solar cells applications have attracted attention in recent years due to their low-cost production and high efficiency. Fig. 23.2 shows the molecular structure of N719, which is an example of a Ru-based dye molecule. As seen in this figure, Ru is located at the center of the molecule and six N atoms are attached to it. Comparing Figs. 23.1 and 23.2, we observe that the local atomic environment around the transition-metal impurity is similar in these two different types of molecules. In Section 23.2.3, we show results from DFT + QMC calculations including interorbital Coulomb interactions and observe that the IBS also exists in the electronic structure of the Ru-based dye molecules.

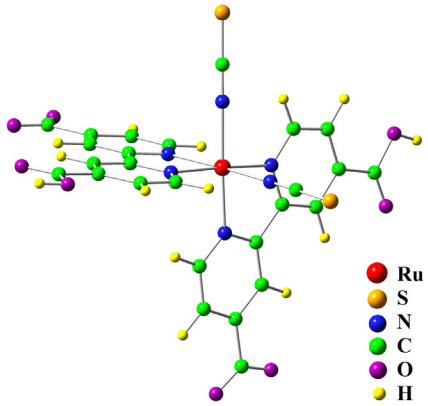

FIGURE 23.2 Molecular structure of the N719 Ru-based dye molecule $[C_{26}H_{14}N_6O_8RuS_2]^{-2}$.

23.1.3 Comparison with the Diluted Magnetic Semiconductors

Vitamin B_{12} and Ru-based dye molecule N719 exhibit energy gaps in their spectrum and contain transition-metal atoms. In this respect, they are similar to an entirely different class of materials that are named as diluted magnetic semiconductors (DMS) [7,8]. The DMS materials are obtained by substituting transition-metal impurities into a semiconductor host. For example, (Ga,Mn)As is obtained by substituting Mn impurities for Ga in the GaAs semiconductor.

DMS materials have attracted much attention because of their magnetic and semiconducting properties. They display high Curie temperatures. In addition, an impurity bound state, which is a sharp resonant state in the single-particle spectrum, exists 110 meV above the top of the valence band in the semiconducting gap [9]. The impurity bound state consists of spectral weight from both the Mn impurity and the host. Calculations performed by using the Haldane–Anderson model show that this new electronic state is important in determining the electronic and magnetic properties of (Ga,Mn)As [10–12]. In particular, long-range ferromagnetic correlations exist among Mn impurities when the chemical potential is located between the top of the valence band and IBS. These ferromagnetic correlations disappear rapidly as the IBS becomes occupied by electrons. Due to these electronic and magnetic properties, the DMS materials have potential for new device applications [13], for example in spintronics [14,15].

When studied within the framework of the Haldane–Anderson model [16], the vitamin B_{12}, the Ru-based dye molecules, and the DMS materials have similar electronic structures; they have semiconducting energy gaps, they contain transition-metal impurities. In addition, we observe that all these different classes of materials have IBS in the electronic spectrum which control the magnetic properties. Hence, we think that the IBS will also play an important role in determining the electronic properties of future artificially-synthesized organic molecules which contain transition-metal atoms.

23.1.4 Haldane–Anderson Model

The Haldane–Anderson model was introduced in order to describe the electronic state of a transition-metal impurity placed in a semiconductor host [16]. In this model, the d orbitals of the transition-metal atom are named as the impurity and the remaining orbitals are named as the host.

In our calculations for metalloproteins, metalloenzymes, and the Ru-based dye molecules, we employ an extended multiorbital single-impurity Haldane–Anderson model which is given by

$$\begin{aligned} H = & \sum_{m,\sigma}(\varepsilon_m - \mu)c^{\dagger}_{m\sigma}c_{m\sigma} + \sum_{\nu,\sigma}(\varepsilon_{d\nu} - \mu)d^{\dagger}_{\nu\sigma}d_{\nu\sigma} \\ & + \sum_{m,\nu,\sigma}(V_{m\nu}c^{\dagger}_{m\sigma}d_{\nu\sigma} + V^{*}_{m\nu}d^{\dagger}_{\nu\sigma}c_{m\sigma}) \\ & + \sum_{\nu} U n_{\nu\uparrow}n_{\nu\downarrow} \\ & + \sum_{\nu>\nu',\sigma}[U' n_{\nu\sigma}n_{\nu'-\sigma} + (U'-J)n_{\nu\sigma}n_{\nu'\sigma}]. \end{aligned} \tag{23.1}$$

Here, $c^{\dagger}_{m\sigma}$ ($c_{m\sigma}$) creates (annihilates) an electron in host state m with spin σ, $d^{\dagger}_{\nu\sigma}$ ($d_{\nu\sigma}$) is the creation (annihilation) operator for a localized electron with spin σ at the impurity d orbital, and $n_{\nu\sigma} = d^{\dagger}_{\nu\sigma}d_{\nu\sigma}$. In addition, ε_m and $\varepsilon_{d\nu}$ are the energies of the host and the d_ν impurity states, respectively, The hybridization matrix element between these states is $V_{m\nu}$. The intraorbital Coulomb repulsion is U. Furthermore, U' and $U'-J$ are the Coulomb interactions between the two d electrons located at different orbitals with opposite and parallel spins, respectively. Here, J is the Hund's coupling term. Finally, a chemical potential μ is introduced since the QMC calculations are performed in the grand canonical ensemble. We note that the Haldane–Anderson model was first used within the Hartree–Fock approximation by [17] for describing the electronic structure of hemoglobin, which is a metalloprotein.

In our calculations for CNCbl molecule, we took the atomic coordinates from the Protein Data Bank [18]. For the Ru-based dye molecule N719, we used the molecular structure given by Ref. [19]. The Anderson model parameters ε_m, $\varepsilon_{d\nu}$, and $V_{m\nu}$ were estimated by using both the HF approximation and the DFT. For the Coulomb parameters U and J we used the well known estimates and also took $U' = U - 2J$.

The resulting extended multiorbital Haldane–Anderson model is studied with the QMC technique developed by Hirsch and Fye [20]. With this technique, we obtain the electron occupancy numbers and the effective magnetic moments for all of the 3d orbitals along with the host orbitals. We also calculate the magnetic correlation functions among the various host and 3d orbitals.

23.2 QUANTUM MONTE CARLO RESULTS ON VITAMIN B_{12} AND THE Ru-BASED DYE MOLECULE N719

23.2.1 HF + QMC Results for Im-[Co^{III} (corrin)]-CN^{+}

We begin by presenting QMC data for the truncated CNCbl structure (Im-[Co^{III} (corrin)]-CN^{+}) [5]. We have performed HF + QMC calculations to obtain the electronic properties of this molecule without including the interorbital Coulomb interaction terms U' and $U'-J$. Here, we study the electronic structure of the Anderson Hamiltonian by varying the chemical potential as a free parameter. Fig. 23.3A shows QMC results on the electron occupation number $\langle n_\nu \rangle$ of the Co($3d_\nu$) orbitals as a function of the chemical potential μ. Similarly, the square of the magnetic moment $\langle (M^z_\nu)^2 \rangle$ at the Co($3d_\nu$) orbitals is shown in Fig. 23.3B as a function of μ. In these figures, the solid black and dashed lines denote the highest occupied molecular orbital (HOMO) level and the lowest unoccupied molecular orbital (LUMO) level found by the HF approximation, respectively.

We observe in Fig. 23.3A that $\langle n_\nu \rangle$ exhibits a jump at $\mu \approx -45$ eV for xz, x^2-y^2, and yz orbitals, because the $\varepsilon_{d\nu}$ values are located near -45 eV for these orbitals. These orbitals remain singly occupied up to $\mu \approx -10$ eV. Near $\mu = -10$ eV they become nearly doubly occupied. We see in Fig. 23.3B that the magnetic moments at xz, x^2-y^2, and yz orbitals have their maximum value at around $\mu = -10$ eV. Above $\mu = -10$ eV, these moments decrease rapidly due to double occupancy of the orbitals.

The situation is different for the xy and $3z^2-r^2$ orbitals. In Fig. 23.3A, we see that $\langle n_\nu \rangle$ for xy and $3z^2-r^2$ orbitals increases rapidly around $\mu \approx -30$ eV where the $\varepsilon_{d\nu}$ values are located. It is important to point out that these orbitals have less than one electron until μ reaches about -5.5 eV, where $\langle n_{xy} \rangle$ exhibits a sudden increase

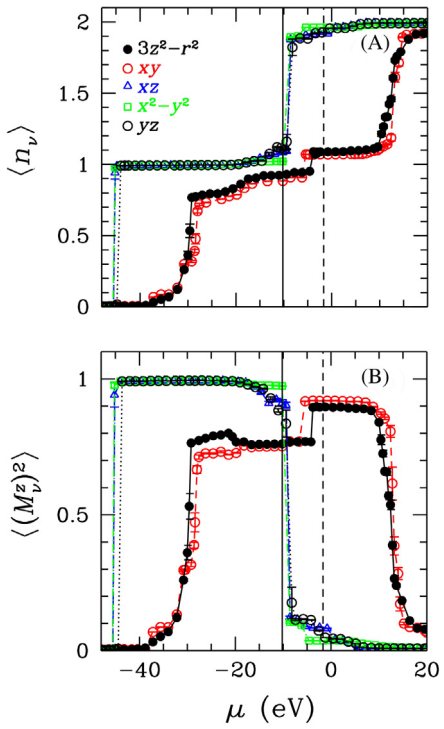

FIGURE 23.3 (A) Electron occupation number $\langle n_\nu \rangle$ of the Co($3d_\nu$) orbitals plotted as a function of the chemical potential μ. (B) Square of the local magnetic moment $\langle (M_\nu^z)^2 \rangle$ at the Co($3d_\nu$) orbitals versus the chemical potential μ. These results are from the HF + QMC calculations for Im-[Co^{III} (corrin)]-CN^+ performed by using $U = 36$ eV. Here, the interorbital Coulomb interactions are ignored. In addition, the vertical solid and dashed lines denote the HOMO and the LUMO levels found by the HF approximation, respectively. *HF + QMC*, Hartree−Fock and quantum Monte Carlo; *HOMO*, highest occupied molecular orbital; *LUMO*, lowest unoccupied molecular orbital.

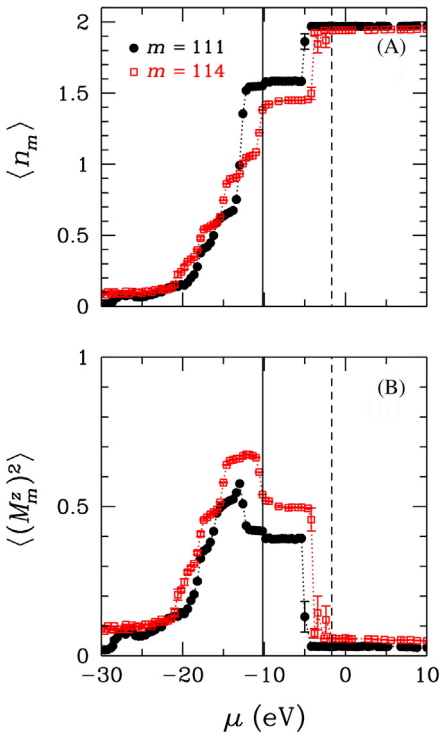

FIGURE 23.4 (A) Occupation of the mth host eigenstate $\langle n_m \rangle$ versus μ. (B) Square of the magnetic moment of the mth host eigenstate $\langle (M_m^z)^2 \rangle$ versus μ. These results are from the HF + QMC calculations for Im-[Co^{III} (corrin)]-CN^+ performed by using $U = 36$ eV. Here, the interorbital Coulomb interactions are ignored. In addition, the vertical solid and dashed lines denote the HOMO and the LUMO levels found by the HF approximation, respectively. *HF + QMC*, Hartree−Fock and quantum Monte Carlo; *HOMO*, highest occupied molecular orbital; *LUMO*, lowest unoccupied molecular orbital.

of about 0.2 electrons. Similarly, for the $3z^2 - r^2$ orbital, a sudden increase occurs at $\mu \approx -4$ eV. It is important to note in Fig. 23.3B that the magnetic moments of the xy and $3z^2 - r^2$ orbitals also increase suddenly at $\mu \approx -5.5$ eV and $\mu \approx -4$ eV, respectively. These sharp increases both in $\langle n_\nu \rangle$ and in $\langle (M_\nu^z)^2 \rangle$ correspond to IBS as found in the Hartree−Fock approximation for the Haldane−Anderson model [10]. Hence, we find that the IBS exists in Im-[Co^{III} (corrin)]-CN^+ at energies -5.5 and -4 eV for the xy and $3z^2 - r^2$ orbitals, respectively. Above $\mu \approx 10$ eV, the xy and $3z^2 - r^2$ orbitals become doubly occupied, and the magnetic moments rapidly decrease.

In Fig. 23.4A and B, we present QMC data on the host electron number $\langle n_m \rangle$ versus μ and the square of the magnetic moment $\langle (M_m^z)^2 \rangle$ versus μ for the $m = 111$ and $m = 114$th host states, respectively. These host orbitals consist mainly of the C(2p) and N(2p) orbitals neighboring the Co atom. Here, we choose these host states because they have the highest hybridization values with the Co($3d_\nu$) xy and $3z^2 - r^2$ orbitals, respectively. Here we observe that, because of hybridization, these host orbitals have partial occupancies and develop magnetic moments. In particular, both $\langle n_\nu \rangle$ and $\langle (M_\nu^z)^2 \rangle$ exhibit sudden increases at the IBS locations, as expected within the HF approximation.

We have also studied the magnetic correlation function $\langle M_\nu^z M_m^z \rangle$ between the Co(3d) electrons and the host states $m = 111$ and $m = 114$ as a function of the chemical potential μ. In Fig. 23.5A, we observe that the xy orbital develops antiferromagnetic (AF) correlations with the $m = 111$th host state. These AF correlations diminish rapidly at $\mu \approx -5.5$ eV. Fig. 23.5B shows similar results for the $3z^2 - r^2$ orbital. In these figures, we observe that AF correlations exist between these host states and 3d orbitals, and that these correlations vanish rapidly as the IBS becomes occupied by electrons.

23.2.2 DFT + QMC Results for CNCbl

The charge neutral CNCbl molecule contains 181 atoms and 718 electrons. In this section, we show the

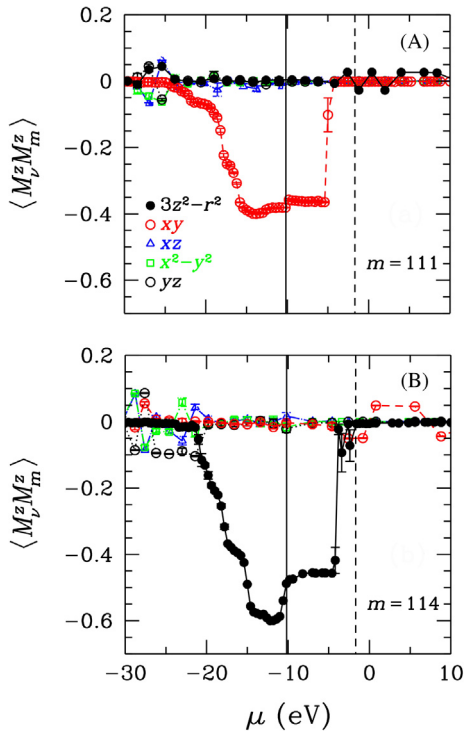

FIGURE 23.5 Magnetic correlation function $\langle M_\nu^z M_m^z \rangle$ between the mth host eigenstate and the various the Co($3d_\nu$) orbitals. Here results are shown for host states (A) $m = 111$ and (B) 114. These results are from the HF + QMC calculations for Im-[Co^{III} (corrin)]-CN^+ performed by using $U = 36$ eV. Here, the interorbital Coulomb interactions are ignored. In addition, the vertical solid and dashed lines denote the HOMO and the LUMO levels found by the HF approximation, respectively. *HF + QMC*, Hartree–Fock and quantum Monte Carlo; *HOMO*, highest occupied molecular orbital; *LUMO*, lowest unoccupied molecular orbital.

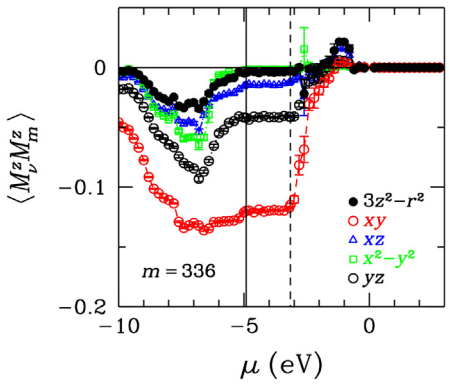

FIGURE 23.6 Magnetic correlation function $\langle M_\nu^z M_m^z \rangle$ between the $m = 336$th host state and the Co($3d_\nu$) orbitals. These results are from the DFT + QMC calculations for the full CNCbl molecule. Here, the intraorbital and interorbital Coulomb interactions were taken into account along with the Hund's coupling. The Coulomb parameters were taken to be $U = 4$ eV and $J = 0.8$ eV. In addition, the vertical solid and dashed lines denote the HOMO and LUMO found by DFT, respectively. *DFT*, density functional theory; *QMC*, quantum Monte Carlo; *CNCbl*, cyanocobalamin; *HOMO*, highest occupied molecular orbital; *LUMO*, lowest unoccupied molecular orbital.

DFT + QMC results for the full CNCbl molecule by including the interorbital Coulomb interactions with the Hund's coupling. We see from DFT + QMC results that the IBS is formed in the CNCbl molecule and its existence is not affected by the presence of the Hund's coupling. Hence, the IBS is a robust feature within this approach.

In our calculations, we find that the vanishing of the AF correlations between the 3d and the host orbitals is the clearest sign for determining the location of the IBS [5,6]. For this reason and space consideration, in this section we only show results on $\langle M_\nu^z M_m^z \rangle$ versus μ for the $m = 336$th orbital which has high hybridization matrix elements. This host state consists mainly of the N(2p) orbitals neighboring the Co atom. Fig. 23.6 shows $\langle M_\nu^z M_m^z \rangle$ versus μ. Here, the black solid line represents the HOMO level and the black dashed line represents the LUMO level obtained by the DFT. We observe in Fig. 23.6 that the AF correlations which occur between the 3d orbitals and the $m = 336$th host orbital disappear when the IBS is occupied with the electrons.

When $\mu = -4.6$ eV, we find that the total electron number is 718. Hence, according to these calculations, the IBS is located about 2 eV above the HOMO level. Consequently, we expect to see the structures in the excitation spectrum of the CNCbl molecule at these energies.

In this section, we have observed the existence of the IBS in the electronic spectrum for CNCbl using three different computational approaches. This indicates that the existence of the IBS for CNCbl is robust within the framework of the Haldane–Anderson model. In particular, the Hund's coupling does not smear the IBS.

23.2.3 DFT + QMC Results for the Ru-based Dye Molecule N719

In this section, we present the DFT + QMC results for the dye molecule N719 of which molecular structure is seen in Fig. 23.2. In these calculations, the interorbital Coulomb interactions along with the Hund's coupling are taken into account.

In this section also we only discuss results on the magnetic correlation function between the Ru($4d_\nu$) orbitals and the host orbital which has the highest hybridization. Fig. 23.7 shows $\langle M_\nu^z M_m^z \rangle$ versus μ for the $m = 150$th host state which consists mainly of the N(2p) orbitals neighboring the Ru atom. Here, we observe that the $m = 150$th host state has strong AF correlation especially with the Ru($4d_\nu$) yz and xz orbitals. These AF correlations vanish at $\mu \approx 3$ eV. Hence, we conclude that an IBS exists at this energy in the dye molecule N719. We think that the

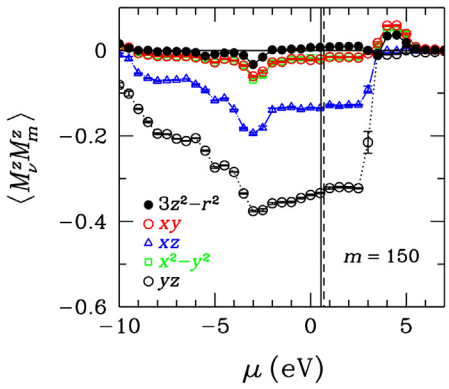

FIGURE 23.7 Magnetic correlation function $\langle M_\nu^z M_m^z \rangle$ between the $m = 150$th host state and the Ru($4d_\nu$) orbitals. These results are from the DFT + QMC calculations for the Ru-based dye molecule N719. Here, the intraorbital and interorbital Coulomb interactions were taken into account along with the Hund's coupling. The Coulomb parameters were taken to be $U = 4$ eV and $J = 0.6$ eV. In addition, the vertical solid and dashed lines denote the HOMO and LUMO found by DFT, respectively. *DFT*, density functional theory; *QMC*, quantum Monte Carlo; *HOMO*, highest occupied molecular orbital; *LUMO*, lowest unoccupied molecular orbital.

IBS found in these calculations might be important for the functioning of the N719 dye molecule.

23.3 SUMMARY AND CONCLUSIONS

In our studies, we have chosen the vitamin B_{12} as an example for metalloenzymes and metalloproteins. For the CNCbl molecule, we have performed HF + QMC and DFT + QMC calculations within an extended multiorbital Haldane–Anderson model including the intraorbital and interorbital Coulomb interactions. We find that the IBS is a robust feature of the electronic spectrum. For example, it is not smeared by the Hund's coupling. We have also seen that the occupancy of the IBS is critical for determining the magnetic properties.

We have performed similar many-body calculations for the dye molecule N719 which contains a Ru atom, in which cases we have also found the existence of the IBS. The results we have found for the IBS in CNCbl and the N719 dye molecule are very similar to what is known about the IBS in the DMS materials. Hence, we have seen that the IBS is a crucial electronic feature of these three very different types of materials.

The artificially- synthesized organic molecules containing transition-metal atoms are interesting because they may lead to important future applications. In the light of the results presented in this article, we expect that the IBS may also play a key role in these new molecules which are yet to be synthesized. In particular, it would be interesting to exploit the properties of the IBS in such molecules with possible applications in electronics, chemical, and pharmaceutical industries.

ACKNOWLEDGMENTS

Financial support by the Turkish Scientific and Technical Research Council (TUBITAK grant numbers 113F242) is gratefully acknowledged.

The numerical calculations reported here were performed in part at the TUBITAK ULAKBIM, High Performance and Grid Computing Center (TRUBA resources).

REFERENCES

[1] J.M. Pratt, Inorganic Chemistry of Vitamin B_{12}, Academic Press, New York, 1972.
[2] B. Krautler, D. Arigoni, B.T. Golding, Vitamin B_{12} and B_{12} proteins, Wiley-VCH Verlag GmbH, Weinheim, 1998.
[3] R. Banerjee (Ed.), Chemistry and Biochemistry of B_{12}, Wiley, New York, 1999.
[4] K.L. Brown, Chemistry and Enzymology of Vitamin B_{12}, Chem. Rev. 105 (2005) 2075.
[5] Z. Kandemir, S. Mayda, N. Bulut, Electronic structure and correlations of vitamin B_{12} studied within the Haldane-Anderson impurity model, Eur. Phys. J. B 89 (2016) 113.
[6] S. Mayda, Z. Kandemir, N. Bulut, Electronic Structure of Cyanocobalamin: DFT + QMC Study, J. Supercond. Nov. Magn. 30 (2017) 3301.
[7] H. Ohno, H. Munekata, T. Penney, S. von Molnar, L.L. Chang, Magnetotransport properties of *p*-type (In,Mn)As diluted magnetic III-V semiconductors, Phys. Rev. Lett. 68 (1992) 2664.
[8] H. Ohno, A. Shen, F. Matsukura, A. Oiwa, A. Endo, S. Katsumoto, Y. Iye, (Ga,Mn)As: A new diluted magnetic semiconductor based on GaAs, Appl. Phys. Lett. 69 (1996) 363.
[9] T. Jungwirth, J. Sinova, A.H. MacDonald, B.L. Gallagher, V. Novak, K.W. Edmonds, et al., Character of states near the Fermi level in (Ga,Mn)As: Impurity to valence band crossover, Phys. Rev. B 76 (2007) 125206.
[10] M. Ichimura, K. Tanikawa, S. Takahashi, G. Baskaran, S. Maekawa, Magnetic impurity states and ferromagnetic interactions in diluted magnetic semiconductors, in: S. Ishioka, K. Fujikawa (Eds.), Foundations of Quantum Mechanics in the Light of New Technology, World Scientific, Singapore, 2006.
[11] N. Bulut, K. Tanikawa, S. Takahashi, S. Maekawa, Long-range ferromagnetic correlations between Anderson impurities in a semiconductor host: Quantum Monte Carlo simulations, Phys. Rev. B 76 (2007) 045220.
[12] Y. Tomoda, N. Bulut, S. Maekawa, Inter-impurity and impurity–host magnetic correlations in semiconductors with low-density transition–metal impurities, Physica B 404 (2009) 1159.
[13] H. Munekata, H. Ohno, S. von Molnar, A. Segmuller, L.L. Chang, L. Esaki, Diluted magnetic III-V semiconductors, Phys. Rev. Lett. 63 (1989) 1849.
[14] S. Maekawa (Ed.), Concepts in Spin Electronics, Oxford University Press, New York, 2006.
[15] I. Žutić, J. Fabian, S.D. Sarma, Spintronics: Fundamentals and applications, Rev. Mod. Phys. 76 (2004) 323.
[16] F.D.M. Haldane, P.W. Anderson, Simple model of multiple charge states of transition-metal impurities in semiconductors, Phys. Rev. B 13 (1976) 2553.
[17] K. Yamauchi, H. Maebashi, H. Katayama-Yoshida, Charge and Spin States of Transition-Metal Atoms in a Hemoprotein Based on the Extended Haldane–Anderson Model, J. Phys. Soc. Jpn. 72 (2003) 2029.
[18] H.M. Berman, J. Westbrook, Z. Feng, G. Gilliland, T.N. Bhat, H. Weissig, et al., Nucleic Acids Res. 28 (2000) 235. Available from: www.rcsb.org.
[19] F. Schiffmann, J. VandeVondele, J. Hutter, R. Wirz, A. Urakawa, A. Baiker, Protonation-Dependent Binding of Ruthenium Bipyridyl Complexes to the Anatase(101) Surface, J. Phys. Chem. C 114 (2010) 8398.
[20] J.E. Hirsch, R.M. Fye, Monte Carlo Method for Magnetic Impurities in Metals, Phys. Rev. Lett. 56 (1986) 2521.